ACS APPLIED MATERIALS & INTERFACES

Research Article

www.acsami.org

Interactive Effect of Hysteresis and Surface Chemistry on Gated Silicon Nanowire Gas Sensors

Yair Paska and Hossam Haick*

The Department of Chemical Engineering and Russell Berrie Nanotechnology Institute, Technion—Israel Institute of Technology, Haifa 32000, Israel

Supporting Information

ABSTRACT: Gated silicon nanowire gas sensors have emerged as promising devices for chemical and biological sensing applications. Nevertheless, the performance of these devices is usually accompanied by a "hysteresis" phenomenon that limits their performance under real-world conditions. In this paper, we use a series of systematically changed trichlorosilane-based organic monolayers to study the interactive effect of hysteresis and surface chemistry on gated silicon nanowire gas sensors. The results show that the density of the exposed or unpassivated Si−OH groups (trap states) on the silicon nanowire surface play by far a crucial effect on the hysteresis characteristics of the gated silicon nanowire sensors, relative to the effect of hydrophobicity or molecular density of the organic monolayer. Based on these findings, we provide a tentative model-based understanding of (i) the relation between the adsorbed organic molecules, the hysteresis, and the related fundamental parameters of gated silicon nanowire characteristics and of (ii) the relation between the hysteresis drift and possible screening effect on gated silicon nanowire gas sensors upon exposure to different analytes at real-world conditions. The findings reported in this paper could be considered as a launching pad for extending the use of the gated silicon nanowire gas sensors for discriminations between polar and nonpolar analytes in complex, real-world gas mixtures.

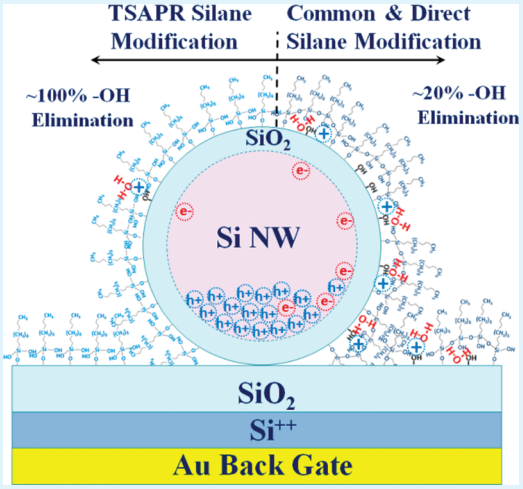

KEYWORDS: *silicon, nanowire, transistor, sensor, hysteresis*

INTRODUCTION

Gated silicon nanowire (Si NW) devices, such as Si NW field effect transistors (FETs), have emerged as promising devices for chemical and biological sensing applications.[1−8] In a standard back gate Si NW FET configuration, the electronic transport through the Si NW is affected by the periphery surfaces, interfaces and/or adsorbed atmosphere molecules near the charge carrier channel.[9−15] Generally, these interactive effects lead to a "hysteresis" phenomenon, namely, a lag in the response obtained in the forward and backward electrical scans of the source-drain current (I_{ds}) vs back-gate voltage (V_{bgs}).[16−23]

The hysteresis effect appears because applying a large gate bias lead to the injection of charge from (into) the Si NW into (from) the Si NW atop (oxide) surface sites, where the charge is trapped until the gate polarity is reversed.[13,18,24] The higher is the environmental humidity or confounding factors, such as those appear in real-world conditions,[25] the higher is the hysteresis and the higher is the screening of the targeted analytes. This essential drawback currently limits the widespread use of Si NW FETs in real-world environmental monitoring, homeland security, quality control in the food industry, medical sensing, and other areas (cf., refs 3 and 26).

It is believed that the Si NW FET hysteresis is caused by surface hydroxyl (Si−OH) sites,[27−29] where water, $Si-O^-$, $Si-OH_2^+$, OH^-, or H^+ species (hereby, surface trap states) originally exist.[13,24,30] These trap states could be removed by thermal passivation,[18,21,22,24] vacuum, or by chemical passivation via direct Si−C bond of nonoxidized Si NWs.[30,31] A conceptually simpler and more cost-effective approach to remove these trap states and the associated hysteresis effect is based on the functionalization of the Si NW's oxide sheath by a monolayer of trichlorosilane (TS) molecules via Si−O−Si bonds.[7,32−36] In this context, it has been believed that the longer is the chain length of the TS molecules or the higher is the molecular density or hydrophobicity of the TS monolayers the lower is the hysteresis effect.[37,38]

Here, we show that the hydrophobicity and/or molecular density of the TS monolayers[35,36] does not necessarily play a crucial role in determining the hysteresis in Si NW FET gas sensors. Rather, we show that the critical effect on the hysteresis of gas Si NW FET sensors[2] is the concentration of the exposed or

Received: February 19, 2012
Accepted: April 23, 2012
Published: April 23, 2012

unpassivated Si−OH groups (trap states) within the adsorbed TS monolayer. We reach this conclusion by a series of surface analysis and electrical measurements of TS molecules whose adsorption characteristics on Si NWs can be changed systematically.[37,38] On the basis of these results, we provide a tentative understanding of (i) the relation between the adsorbed TS molecules, the hysteresis, or the fundamental parameters of FETs (including threshold voltage, carrier mobility, subthreshold swing, off-current, off-voltage) and of (ii) the relation between the hysteresis drift and possible screening effect on Si NW FET sensors upon exposure to different analytes at real-world conditions. The implications of the obtained results are presented and discussed in the text.

EXPERIMENTAL SECTION

Synthesis, Fabrication, and Functionalization of the Si NWs. The synthesis of the Si NWs,[39] as well as the fabrication of Si NW FETs[1,2] (Figure 1a and b), were described earlier. Briefly, p-type (112)

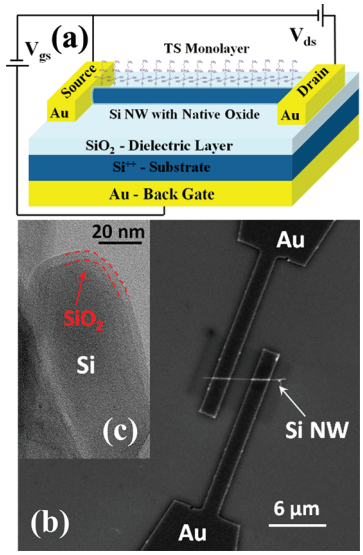

Figure 1. (a) Schematics of a back-gate Si NW FET configuration, coated with TS monolayer; (b) scanning electron microscopy (SEM) image of a representative Si NW FET; and (c) transmission electron microscopy (TEM) image of a representative Si NW (~50 ± 5 nm in diameter) having ~5 ± 1 nm native oxide on its surface.

Si NWs doped with boron to a doping level of $\sim 10^{16}$ cm^{-3} were prepared by the vapor−liquid−solid growth technique. Transmission electron microscopy (TEM) analysis indicated that these Si NWs consisted almost entirely of smooth Si cores (50 ± 5 nm in diameter) that are coated with ~5 ± 1 nm native SiO_2 layer (see Figure 1c).

Individual Si NWs were contacted by a source and drain Au/Ti electrodes (10 nm Ti and 100 nm Au) that are mutually separated by 2 μm on top of a 100 nm thermally oxidized degenerately doped p-type Si (0.001Ω·cm resistivity) substrate (see Figure 1a).[1,2] The obtained devices were functionalized with a series of trichlorosilane (TS) monolayers, differing by their carbon chain length, $CH_3(CH_2)_nSiCl_3$ (with $n + 1 = 3, 6, 8, 12, 18$), using "two-step amine promoted reaction" (TSAPR).[1,2,37,40,41] A simplified scheme and a brief description of the TSAPR procedure is presented in Figure 2. In few instances, TSAPR-made TS monolayers were compared with TS monolayers prepared by the commonly used *direct self-assembly*[27] procedure. A simplified scheme and a brief description of the *direct self-assembly* procedure is presented in the Supporting Information, Figure 1S.

Si NW FET Measurements and Exposure to Analytes. A probe station that is connected to a device analyzer (Agilent B1500A) was used to collect the electrical signals of the Si NW FETs before and after exposure to analytes. Source-drain current (I_{ds}) versus voltage dependent back-gate (V_{bgs}) measurements, swept backward and forward between +40 V to −40 V with 200 mV steps and at 1 V source-drain voltage (V_{ds}) and a sweep rate of 3.2 V/s, were carried out as follows:

(i) after a sequential process of 1 min precleaning by di-ionized water, 5 min sonication with chloroform, and 12 h drying in 110 °C vacuum oven (hereafter, OH^{low});
(ii) after 2 min ultraviolet-ozone cleaning (UVOCs) that enriches the Si NW oxide surface with Si−OH groups (hereafter, OH^{high});
(iii) after modification with controlled, TSAPR-made TS monolayer (hereafter, TS^c) or after *uncontrolled*, direct self-assembly[27] of TS monolayer (hereafter, TS^{uc}); and
(iv) upon exposure of the OH^{low}-, OH^{high}-, T^{Sc}-, and TS^{uc}-modified Si NW FETs to different concentrations of nonpolar and polar analytes (see Table 2) or humidity conditions.

Each of the sequential four steps were first monitored under a flow of reference air (15% relative humidity (RH) and <0.3 ppm organic contaminants). For step-iv, exposure to different analytes or humidity conditions was accomplished by passing the reference air through a glass bubbler containing a liquid phase of the analyte of interest (purchased from Sigma Aldrich Ltd. and Fluka Ltd.; >99% purity; <0.001% water). The air emitted from the bubblers, mostly under saturation conditions, was diluted (with a total average flow of 5 L min^{-1}) with the reference air to reach lower levels of analyte concentrations or humidity conditions. In this way, the system was able to regulate the analyte concentration levels between 1 ppm to 200 ppm and the RH levels between 15% and 80%. The concentration levels of analytes were measured by a commercial photoionization detector (ppbRAE 3000; Rae Systems, US) with a detection limit of ~10 ppb. Each experiment was repeated on four devices from different Si NW batches.

Ellipsometry Measurements. Planar Si(111) substrates with 1.7 ± 0.3 nm native oxide were coated with TS^c monolayers (hereafter, TS^c-Si(111)) in the same way as the Si NWs. A variable angle rotating compensator spectroscopic ellipsometer (M-2000 V, J. A. Woollam Co., Inc.) was used to determine the exact thickness of the native oxide layer at five incidence angles (60°, 65°, 70°, 75°, 80°) on an open sample stage, prior to the TS^c functionalization, using tabulated values for the refractive indices of Si and SiO_2. The thickness and refractive index of the TS^c monolayers were determined from multiangle spectroscopic ellipsometry measurements on an open sample stage. The ellipsometric angles were recorded over a spectral range of 250−1700 nm and a three-phase TS^c/(native-SiO_2)/Si substrate model was used to extract the electronic contribution to the wavelength (λ) dependent refractive index (n) and the thickness of the TS^c monolayers (d_{TS}). The electronic part of the refractive index (n_∞) was extrapolated ($\lambda \rightarrow \infty$) from $n(\lambda)$ in the ultraviolet−near-infrared (UV-NIR) spectral region, and squared to obtain the TS^c monolayer electronic dielectric constant (ε_{TS}). Each experiment was repeated on three samples and with three measurement points on each sample.

Kelvin Probe Measurements. The work function of TS^c-Si(111) surfaces ($\Phi_{TS\text{-}Si(111)}$) were determined by Kelvin probe. (KP Technology Ltd., UK). The Kelvin probe package includes a head unit with an integral tip amplifier, a 2 mm tip, a PCI data acquisition system, a digital electronics module, a system software, an optical baseboard with sample and Kelvin probe mounts, and a 1 in. manual translator, all placed inside a Faraday cage. The work function resolution of the system is 1−3 mV. The Kelvin probe technique measures the contact potential difference between a vibrating reference Au probe (Φ_{Au} = 5.1 eV) and the sample. The contact potential difference is defined as the difference in the work function of the two surfaces ($\Delta\Phi = \Phi_{TS\text{-}Si(111)} - \Phi_{Au}$). Typically the contact potential difference was extracted after a saturation of 1000 measurements points (~30 min). Each experiment was repeated on three samples and with three measurement points on each sample.

X-ray Photoelectron Spectrometry. Chemical surface analysis of TS^c-Si(111) surfaces was performed by X-ray photoelectron spectroscopy (XPS; Thermo VG Scientific, Sigma probe, England)

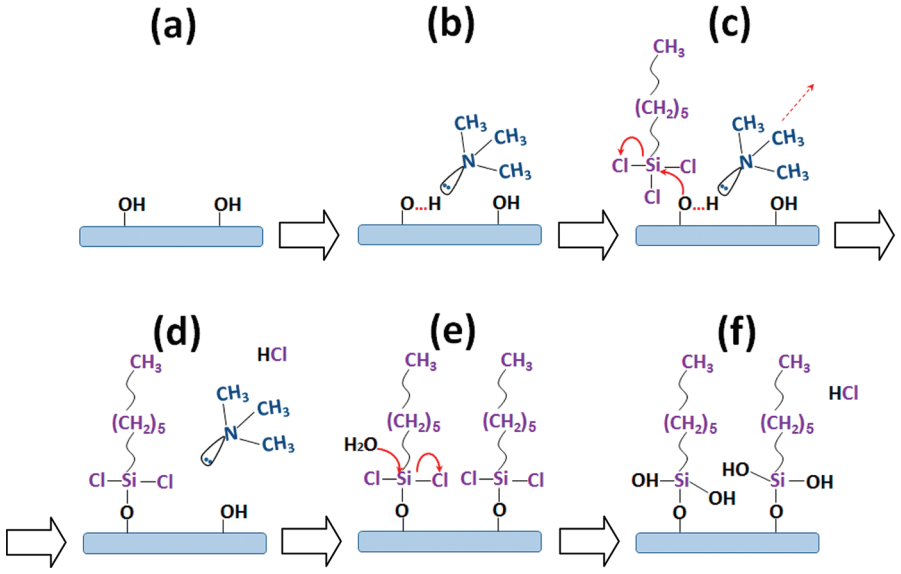

Figure 2. Simplified scheme for the attachment of hexyltrichlorosilane (HTS), as a representative example for TS monolayers, to SiO_2/Si surface by the TSAPR procedure: (a) SiO_2/Si surface with free hydroxyl (Si−OH) groups is prepared (a) and exposed to trimethylamine (TMA) gas for a period of 6 min, to form a hydrogen bond with the Si−OH group and to make the oxygen atom more nucleophilic. The TMA-treated SiO_2/Si surface is then exposed to 1.5 mM HTS in a chloroform solution for 1 h (c). At this stage, the oxygen atom of the Si−OH group attacks the HTS's silicon atom and form Si−O−Si bond (d). The presence of water residues assists the replacement of HTS's chlorine atoms by OH groups (e). At the end of this reaction, the samples are sonicated in chloroform for 5 min to remove physically adsorbed TS residues, leading to a monolayer of noncrossed HTS on the SiO_2/Si surface (f).

Table 1. XPS's Peak Position and Peak Areas of TS^c Monolayers, $CH_3(CH_2)_nSiCl_3$, with Different Carbon Chain Length

	peak area (au)								
chain length of TS^c	Si 2p 3/2 (99.3 ± 0.02 eV)	Si 2p 1/2 (99.9 ± 0.02 eV)	Si 2p Si_2O (100.27 ± 0.02 eV)	Si 2p SiO (101.07 ± 0.02 eV)	Si 2p Si_2O_3 (101.8 ± 0.02 eV)	Si 2p R-SiO_3 (102.58 ± 0.02 eV)	Si 2p SiO_2 (103.35 ± 0.02 eV)	C 1s C−C (285.15 ± 0.02 eV)	C 1s C−O (288 ± 0.02 eV)
$n + 1 = 3$	1075 ± 8	537 ± 2	46 ± 1	17 ± 1	18 ± 1	177 ± 2	1000 ± 10	978 ± 15	41 ± 2
$n + 1 = 6$	1071 ± 8	536 ± 2	46 ± 1	16 ± 1	18 ± 1	170 ± 2	1000 ± 10	2207 ± 15	78 ± 2
$n + 1 = 8$	1056 ± 8	533 ± 2	45 ± 1	17 ± 1	18 ± 1	149 ± 2	1000 ± 10	1437 ± 15	75 ± 2
$n + 1 = 12$	998 ± 8	529 ± 2	46 ± 1	16 ± 1	17 ± 1	133 ± 2	1000 ± 10	1620 ± 15	42 ± 2
$n + 1 = 18$	788 ± 8	394 ± 2	46 ± 1	17 ± 1	18 ± 1	89 ± 2	1000 ± 10	3105 ± 15	91 ± 2

having a base pressure of $<3 \times 10^{-9}$ Torr and fitted with a monochromatized Al Kα (1486.6 eV) X-ray source. The measurements were performed in the surface and bulk-sensitive modes at 14.5° and 59.5° takeoff angle between the direction of the analyzer and the specimen plane, respectively. All measurements were taken on the center of the sample to ensure reproducibility and to minimize the effects of scratches or contamination at the edges. A bare Si(111) surface with 1.7 ± 0.3 nm native oxide was used as a reference. Samples were first scanned from 0 to 1000 eV to monitor signals for Si, C and O. The Si2p region at 98−105 eV and the C1s region at 282−287 eV were investigated in detail. Spectral analysis was performed using the peak fitting software (XPSPEAK version 4.1) after a Shirley background subtraction. The spectra were first fit to a Shirley background, which was then subtracted to allow peak fitting. The spectra were then deconvoluted using 10% ratio Lorentzian−Gaussian peaks. For Si 2p spectra six peaks were fitted. The shift of each signal relative to the Si $2p_{3/2}$ (99.30 ± 0.02 eV) signal is listed in parentheses close to the peak's name: Si $2p_{1/2}$ (+0.60 ± 0.02 eV), Si_{2p} Si_2O (+0.97 ± 0.02 eV), Si_{2p} SiO (+1.77 ± 0.02 eV), Si_{2p} Si_2O_3 (+2.50 ± 0.02 eV), Si_{2p} SiO_2 (+4.05 ± 0.05 eV) and Si_{2p} R-SiO_3 (+3.28 ± 0.05 eV) that originate from the TS^c binding group (see Table 1). The ratio between the Si $2p_{1/2}$ to Si $2p_{3/2}$ peak areas was fixed at 0.51. For C 1s two peaks were fitted as follows: C_{1s} C−C (285.15 ± 0.02 eV) that originates mostly from the TS^c carbon chain and C_{1s} C−O (288 ± 0.02 eV) that originates from carbon impurities. The spectra were then charge corrected to the Si $2p_{3/2}$ signal (99.30 ± 0.02 eV). The analysis was carried out by extracting the Si $2p_{3/2}$, C_{1s} C−C and Si_{2p} R-SiO_3 peak areas (see Table 1) and by normalizing these areas by the Si_{2p} SiO_2 peak area. In the current paper, the ratio between the Si $2p_{3/2}$ and Si_{2p} SiO_2 peak areas is signed as $r_{Si3/2}$, the ratio between the C_{1s} C−C and Si_{2p} SiO_2 peak areas is signed as r_C, and the ratio between the Si_{2p} R-SiO_3 and Si_{2p} SiO_2 peak areas is signed as $r_{R\text{-}SiO3}$. The Si_{2p} SiO_2 peak area was chosen for normalization, because the native SiO_2 layer is identical for all samples and fully seen by the XPS technique. In contrast, the C_{1s} C−C peak area depends on the TS chain length and the Si $2p_{3/2}$ peak depends on the TS^c monolayer thickness. Each experiment was repeated on three samples and with three measurement points on each sample.

Contact Angle. Static contact angle of TS^c-Si(111) surfaces (θ_{TS}) were obtained with the sessile drop method[42] using a 034451Tamron and ComputarMLH-X10 magnifying lens, attached to a high-resolution U-eye digital camera that was aligned perpendicularly above the surface. For calibration of the pixel size, a small cylinder of precisely known diameter and of the same thickness as that of the sample was used. The pictures were processed with the Image-Pro Plus program, version 4.0 (Media Cybernetics). Several sessile water axisymmetric drops (50 μL) were dispensed on the same sample with the help of a precision microsyringe and then gently shaken for 15 s. The magnitudes of amplitude and frequency of the vibrating plate were usually around 0.2 mm and 13 Hz, respectively. Using the

maximum diameter, drop volume, and the surface tension of water as input values, the θ_{TS} values were then calculated, by fitting into solutions of the Young- Laplace equation, with an accuracy of 0.1°. Each experiment was repeated on three samples and with three measurement points on each sample.

RESULTS

The overall experimental strategy used in the current study is shown in Figure 3. Briefly, each Si NW FET was precleaned

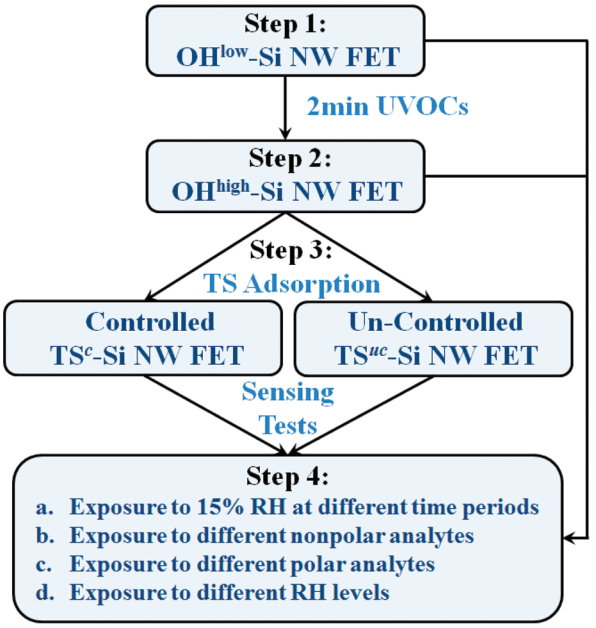

Figure 3. Flowchart of the various sequential steps used to investigate the hysteresis effect on the electrical and sensing properties of the Si NW FETs.

and measured **before** Si−OH enrichment treatment (hereafter, **OH^{low}-Si NW FET**), **after** Si−OH enrichment treatment using UVOCs (hereafter, **OH^{high}-Si NW FET**),[41,47] after modification with TS^c monolayer (hereafter, **TS^c-Si NW FET**),[37,38] and after modification with TS^{uc} monolayer (hereafter, **TS^{uc}-Si NW FET**);[27−29] see Figure 4. The Si NW FETs were then tested electrically before and after exposure to various analyte conditions as well as to various RH conditions, to resemble real-world confounding factors; see Table 2.[1,2,25]

Characterization of TS^c-Si Surfaces. In principle, characterization of Si NWs by XPS and Kelvin probe is possible.[43−45] However, these measurements involve the use of a highly dense array of Si NWs that are not necessarily uniform in their native oxide thickness or in their characteristics.[34] In contrast to XPS and Kelvin probe, spectroscopic ellispsometry and contact angle characterization of Si NWs are still technically challenging. Since this is so, surface analysis of the TS^c monolayers were carried out on top of (native) SiO_2/Si(111) planar substrates.

Figure 2S of the Supporting Information presents the raw and fitted XPS data of the various TS^c-Si(111) surfaces examined in the current study. The calculated $r_{Si3/2}$, r_C, and $r_{R\text{-}SiO3}$ values for the various TS^c-Si(111) surfaces are summarized in Figure 5. As seen in the figure, the $r_{Si3/2}$ values decreased with the increase in TS^c carbon chain length (Figure 5a). This is because the Si $2p_{3/2}$ peak intensity decreased with the increase of the TS^c monolayer thickness, due to the reduction in the

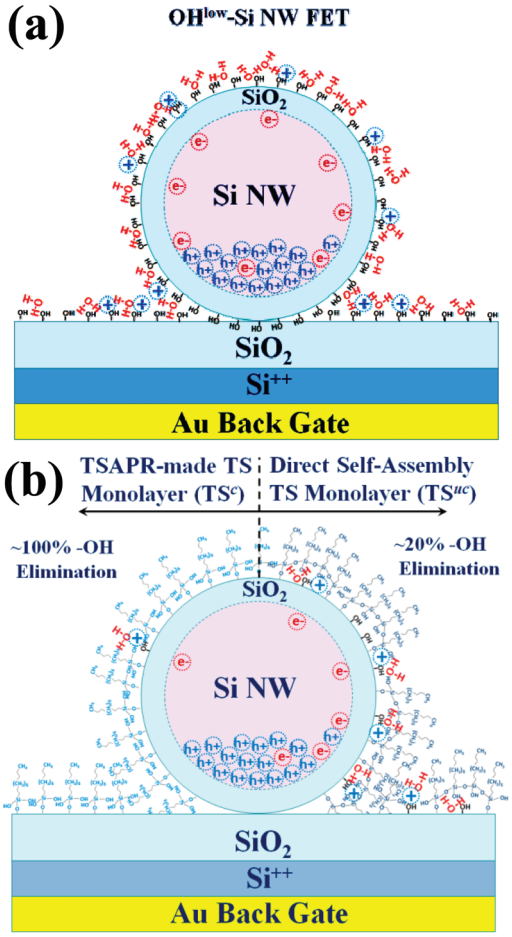

Figure 4. Cross-section schematics of (a) a back-gate OH^{low}-Si NW FET and (b) a back-gate TS^c-Si NW FET (left side) or TS^{uc}-Si NW FET (right side).

Table 2. Physical Properties of the Analytes Used for the Exposure Experiments

analyte	formula	p_o[a] (Torr)	k[b]	dipole (D)	volume (Å^3)
octane	$CH_3(CH_2)_6CH_3$	14	1.94	0	146.6
decane	$CH_3(CH_2)_8CH_3$	1.4	1.98	0	180.2
water	H_2O	32	80.1	1.85	19.3
ethanol	CH_3CH_2OH	59	25.3	1.66	54.0
butanol	$CH_3(CH_2)_3OH$	4	17.8	1.68	87.6

[a] p_o stands for the analyte's vapor pressure at 25 °C. [b] k stands for the dielectric constant of the analyte at 20 °C.

width of the nonoxide Si layer seen by the XPS. The r_C values increased with the increase in the TS^c carbon chain length (Figure 5b). Surprisingly, hexyltrichlorosilane (HTS^c) had a higher r_C value than expected, indicating that HTS^c monolayer has a higher molecular density than the other TS^c molecules. The $r_{R\text{-}SiO3}$ values decreased with the increase in the TS^c carbon chain length (Figure 5c).

The thickness of the TS^c monolayers (d_{TS}), as measured by spectroscopic ellipsometry, increased with the increase in the TS^c carbon chain length (Figure 6a). The carbon packing density of the TS^c monolayers, as measured via the water/TS^c-Si(111) contact angle (θ_{TS}), increased with the increase of TS^c carbon chain length (Figure 6b). HTS^c had higher θ_{TS} value than the expected, most probably due to the higher carbon

dx.doi.org/10.1021/am300288z | ACS Appl. Mater. Interfaces 2012, 4, 2604−2617

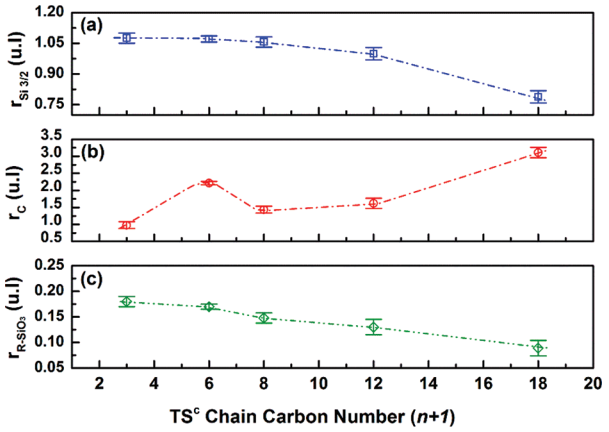

Figure 5. (a) The ratio between the Si $2p_{3/2}$ and Si_{2p} SiO_2 peak areas ($r_{Si3/2}$); (b) the ratio between the C_{1s} C−C and Si_{2p} SiO_2 peak areas (r_c); and (c) the ratio between the Si_{2p} R-SiO_3 and Si_{2p} SiO_2 peak areas ($r_{R\text{-}SiO3}$) for a series of TS^c-Si(111) samples. Each experiment was

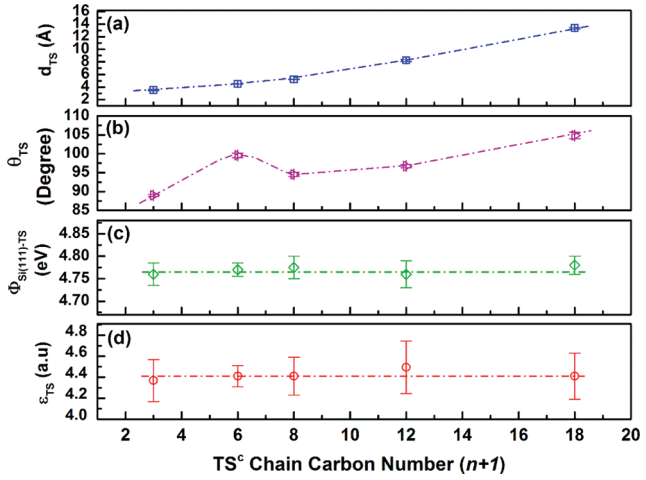

Figure 6. Surface analysis of the TS^c monolayers as a function of the TS chain length: (a) TS^c monolayer thickness (d_{TS}), (b) water contact angle on TS^c-Si(111) substrates, (c) TS^c monolayer dielectric constant (ε_{TS}), and (d) work function of TS^c-Si(111) substrates ($\Phi_{TS\text{-}Si(111)}$). Each experiment was repeated on three samples and with three measurement points on each sample.

content. The work function of the TS^c-Si(111) samples, $\Phi_{TS\text{-}Si(111)}$, and the dielectric constant of the TS^c monolayers (ε_{TS}) exhibited almost the same value ($\Phi_{TS\text{-}Si(111)}$ = 4.77 ± 0.03 eV; ε_{TS} = 4.41 ± 0.25) for all TS chain lengths (see Figures 6c and 6d). Overall, it seems that the electrostatic properties of all five TS^c monolayers under 15% RH are identical to each other.

Electrical and Sensing Characterization of TS^c-Si NW FETs. Figure 7 shows the threshold voltage gap (ΔV_H),[19,22,46] namely, the difference between the threshold voltage (V_{th}) of the backward and the forward source-drain current (I_{ds}) versus back-gate voltage (V_{bgs}) scans, of the various TS^c-Si NW FETs. **Note:** ΔV_H is widely accepted as a measure for the hysteresis.[19,22,46] As seen in the figure, different TS^c monolayers led to different ΔV_H values, with a minimum value (1 ± 0.2 V) at a chain length that is equivalent to TSAPR-made hexyltrichlorosilane (HTS^c; *n+1* = 6). Since minimum ΔV_H means smallest hysteresis or highest surface passivation, we have

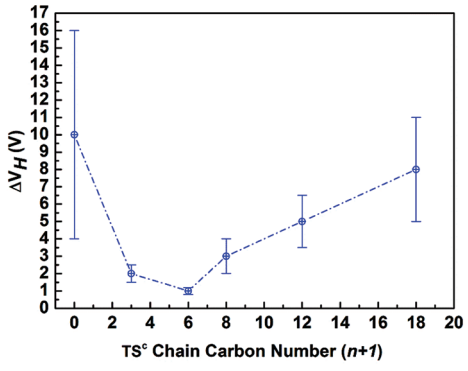

Figure 7. Threshold voltage gap (ΔV_H) of TS^c-Si NW FETs as a function of the TS chain length. The value at 0 represents the ΔV_H of the OH^{low}-Si NW FETs. The results are based on 20 devices in total (all were measured first as OH^{low}-Si NW FET) and on 4 devices for each TS^c modification. These measurements were carried out under 15% RH, V_{ds} = 1 V, and total backward and forward scan time of 25 s per direction (0.06 s per point with 200 mV step).

chosen to focus the presentation of our results and discussion on the HTS^c case and, for fair comparison, on the HTS prepared by the *direct self-assembly* procedure (hereafter, HTS^{uc})

Figure 8 shows the I_{ds}−V_{bgs} characteristics, scanned forward and backward, of a typical test device. As seen in the figure,

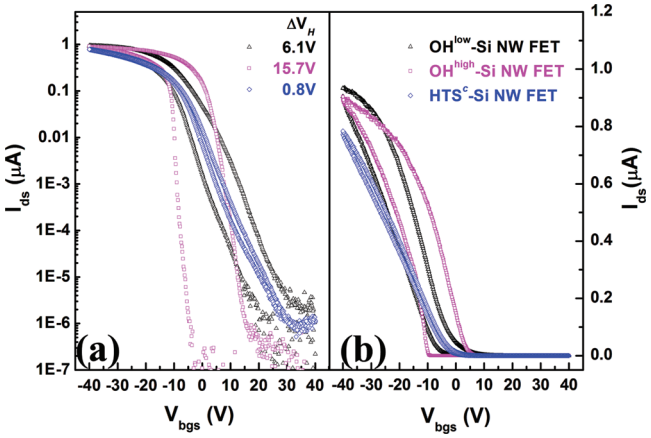

Figure 8. (a) Logarithmic and (b) linear I_{ds}−V_{bgs} characteristics of OH^{low}-Si NW FET, OH^{high}-Si NW FET, and HTS^c-Si NW FET. The measurements were carried out under 15% RH, V_{ds} = 1 V, and a total backward and forward scan time of 25 s per direction (0.06 s per point with 200 mV step). Similar results were obtained, within ±20% experimental error, from the other three duplicates that were prepared from different Si NW batches.

OH^{low}-Si NW FET under 15% RH exhibited I_{ds}−V_{bgs} response that is characteristic to *p*-channel FET, with ΔV_H of about 6.1 V. Typically, this behavior was not stable and continued to change over time (see Supporting Information, Figure 3S). OH^{high}-Si NW FET exhibited ΔV_H of about 15.7 V. This hysteresis (or ΔV_H) was reduced almost completely to about 0.8 V after modifying the device with HTS^c.[2,37] The I_{ds}−V_{bgs} of the HTS^c-Si NW FET response after ~15 min remained stable (see Supporting Information, Figure 5S, inset) and was restorable after each exposure for an overall period of 6 months (not shown). In contrast to the HTS^c-Si NW FET, the hysteresis dynamics of the HTS^{uc}-Si NW FET was widened from 0.8 V to ~11 V after 2 h exposure to 15% RH (see Supporting Information, Figures 4S). All exposures after the 2-h period showed a stable but

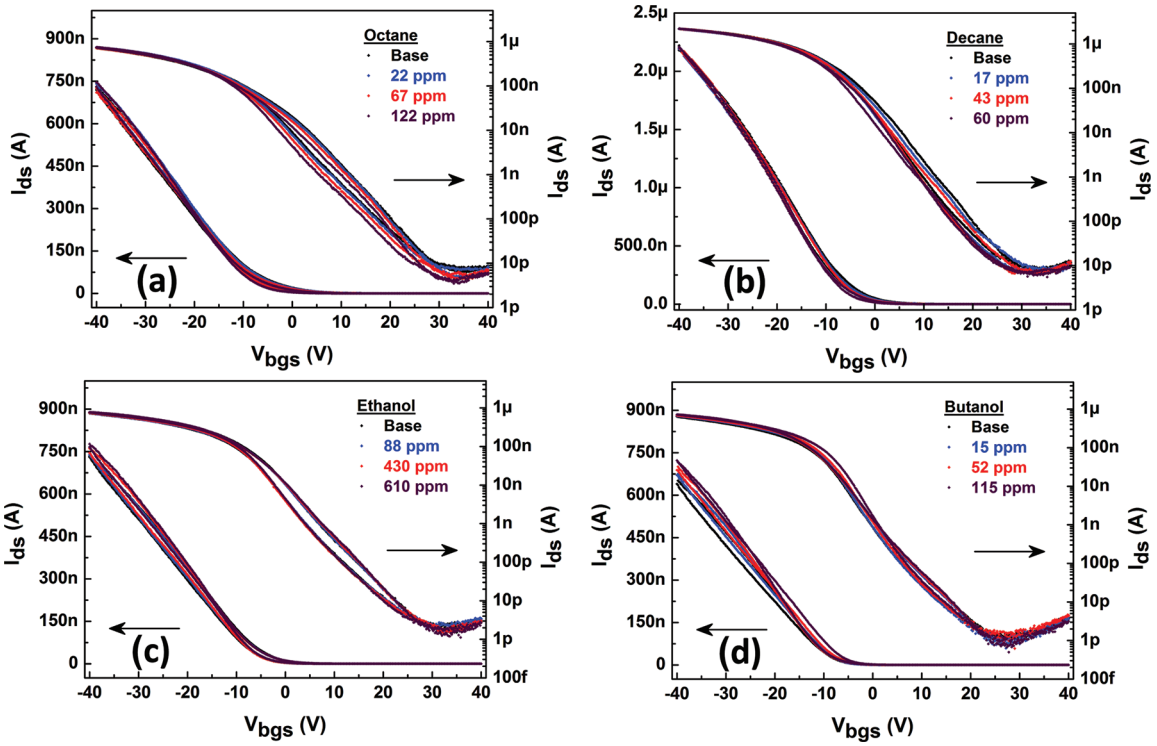

Figure 9. Linear scale (left-axis) and log scale (right-axis) forward and backward $I_{ds}-V_{bgs}$ characteristics response of four different HTS^{c}-Si NW FETs, prepared from different Si NW batches, under (a) 17, 43, and 60 ppm decane; (b) 22, 67, and 122 ppm octane; (c) 88, 430, and 610 ppm ethanol; and (d) 15, 52, and 115 ppm butanol. Similar results were obtained, within ±20% experimental error, from the other three duplicates.

higher (~11 V) hysteresis extent. To quantify the hysteresis, the following relationship was used:

$$qQ_{trap} = \frac{C_{box}|\Delta V_H|}{2\pi r_{nw} L_{nw}} \quad (1)$$

$$\frac{C_{box}}{L_{nw}} = \frac{2\pi\varepsilon_{box}}{\ln\left(\frac{2d_{box}+r_{nw}}{r_{nw}}\right)} \quad (2)$$

Q_{trap} is the number of occupied trap charges; C_{box} is the back-gate capacitance; d_{box} is the width of the gate oxide; ε_{box} is the dielectric constant of the oxide; q is the elementary charge of electron; and L_{nw} and r_{nw} are the length and radius of the Si NW, respectively. On the basis of eqs 1 and 2, the amount of traps in OH^{low}-Si NW FET is evaluated as 1.8×10^{12} cm^{-2}. This number increased to 4.6×10^{12} cm^{-2} in the case of OH^{high}-Si NW FET, but significantly decreased to 2.4×10^{11} cm^{-2} after HTS^{c} modification, indicating that approximately 95% of the traps were passivated due to the HTS^{c} modification.

Traditionally, there are four classes of trap states that could affect the performance of (Si NW) FETs: (i) fixed oxide charge in the bulk, (ii) mobile ionic charge that stem form a contamination, (iii) oxide-trapped charge near an interface, and (iv) interface-trapped charge.[47] Trap states that exist ~5 nm near the SiO_2/Si interface of the Si NW or near the buried oxide interface of the gate (Q_{trap}) affect the hysteresis if they communicate and exchange charge with the Si channel.[48] These traps are considered "slow traps" if they exhibit switching times greater than 1 s. The same traps are considered "fast traps" if they exhibit switching times between 10^{-6} and 1 s.[49] Though the interface trap states have significant effect on the electrical performance of the FETs[12,14] they have much less significant effect on the hysteresis.[48,49] Trap states, such as Si–OH, that are located on top of the Si NW's native oxide can communicate directly with the underlying Si channel, with ***slow*** rates, thus contributing to hysteresis. Therefore, it is reasonable that the changes in $I_{ds}-V_{bgs}$ seen in Figure 8 originate from trap states on the Si NW native oxide surface.

Figure 9 shows the $I_{ds}-V_{bgs}$ characteristics, scanned forward and backward, for four typical test HTS^{c}-Si NW FETs, prepared from different batches, during an exposure to different analytes: (i) decane and octane, as representative noninteracting nonpolar analytes (Figures 9a and 9b) and (ii) ethanol and butanol, as representative interacting polar analytes (Figures 9c and 9d) under 15% RH. For each analyte concentration, the response of the HTS^{c}-Si NW FETs reached a stable response after a relatively short exposure period (less than 15 min). As seen in the figure, HTS^{c}-Si NW FET exhibited very good sensitivity toward nonpolar analytes (cf. ref.[1,2]) and negligible hysteresis drift over the exposure time. The same device responded to polar analytes with small hysteresis drift during the exposure process. For the sake of comparison, the OH^{low}-Si NW FET, OH^{high}-Si NW FET, and HTS^{uc}-Si NW FET exhibited unstable electrical characteristics over time on exposure to reference air with 15% RH. At long exposure periods, these devices exhibited no changes in their electrical characteristics, neither upon exposure to 15% RH nor upon exposure to nonpolar analytes.[1,2] On the other hand, exposing the same devices to polar analytes resulted in unstable (or drifty) responses over time (see Supporting Information, Figure 3S and 4S). The hysteresis under these conditions was significantly higher than that for the HTS^{c}-Si NW FET toward the same polar analytes and concentrations.

Figure 10 shows the $I_{ds}-V_{bgs}$ characteristics, scanned forward and backward, of a typical test HTS^{c}-Si NW FET device during exposure to different RH conditions. As seen in the figure, the

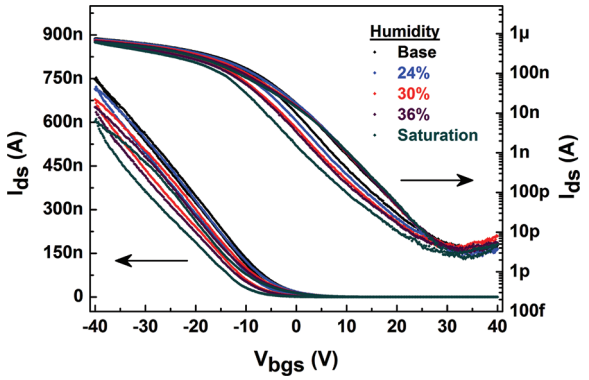

Figure 10. Linear scale (left-axis) and Log scale (right-axis) forward and backward $I_{ds}-V_{bgs}$ characteristics of representative HTS^c-Si NW FET device under 15% (base), 24%, 30%, 36%, and saturation (~80% RH). Similar results were obtained, within ±20% experimental error, from the other three samples that were prepared from different Si NW batches.

$I_{ds}-V_{bgs}$ hysteresis of the HTS^c-Si NW FET device was dependent on the RH level. For example, increasing the humidity from 15% to 36% increased the ΔV_H from 1 V to 1.6 V. At 60%−80% RH, where a film of condensed water was seen on the surface, theΔV_H was increased from 1.6 V to 2.1 V. For each RH level, the HTS^c-Si NW FET device reached a stable response and low hysteresis after a relatively short exposure time (less than 30 min), compared to the responses of the OH^{low}-Si NW FET or the HTS^{uc}-Si NW FET.

DISCUSSION

TS^{uc} monolayers have been used for more than three decades as passivation layers for (native) SiO_2/Si surfaces.[37,38] These monolayers are condensed on the Si surface after the TS molecules have hydrolyzed by water that exist either in the TS solution and/or on the (native) SiO_2-coated Si surface (cf. Supporting Information, Figure 1S).[27−29,36] The result is a two-dimensional polysiloxane network formed by a covalent Si−O−Si bond between adjacent TS molecules and covalent Si−O−Si surface bonds (see Figure 4b, right side; and Supporting Information, Figure 1S).[27−29]

Using various surface analysis techniques, it has been shown that TS^{uc} monolayers of short chains ($n + 1 < 6$) exhibit low packing densities. TS^{uc} monolayers of long chains ($n + 1 > 6$) exhibit high packing densities that are slightly less than the density of crystalline hydrocarbons. For both short and long TS^{uc} chains, **only 10−20%[27−29] of the Si−OH sites** that exist on the (native) SiO_2/Si surface are passivated.[35,36] The result is TS^{uc}-terminated surfaces with plenty of free (unreacted) Si−OH groups that are prone to interaction with water molecules.

Similar to the TS^{uc} monolayer, the higher the TS^c chain length the higher the packing density and the higher the hydrophobicity of the TS^c monolayer (*see* Figure 5b and 6b). However, in comparison to the TS^{uc} monolayers, the TS^c process eliminates higher amounts of free (unreacted) Si−OH groups on the (native) SiO_2/Si surface. For example, the packing density of HTS^c (~3 molecules per ~3 Si−OH groups) is lower than the HTS^{uc} (~5 molecules per ~3 Si−OH groups). However, the HTS^c eliminates ~5 times more hydroxyl groups on the SiO_2/Si surface than the HTS^{uc}. The packing density of controlled, TSAPR-made ocatadecyeltrichlorosilane (OTS^c; 2 molecules per 3 Si−OH groups) is lower than the packing density of uncontrolled, *direct self-assembled* OTS (OTS^{uc}; ~5 molecules per 3 Si−OH groups).[29,36] However, compared to OTS^{uc}, OTS^c eliminates ~4 times more hydroxyl groups on the Si surface.

In the following, we use a model-supported analysis,[1,50] to discuss the effect of hysteresis on the fundamental parameters of the various Si NW FET samples. To understand the effect of the trapped charge on the Si NW surface (hysteresis effect), the $I_{ds}-V_{bgs}$ forward scan of each curve (with the effect of the tapped charges) was compared to the $I_{ds}-V_{bgs}$ backward scan curve (without the effect of the tapped charges); see Figure 8. To understand the effect of Si−OH groups and of the HTS^c modification, the $I_{ds}-V_{bgs}$ backward scans of the OH^{high}-Si NW FET and HTS^c-Si NW FET were compared to the $I_{ds}-V_{bgs}$ backward scans of the OH^{low}-Si NW FETs. For each backward or forward scan the transconductance (g_m) was extracted by $g_m = dI_{ds}/dV_{bgs}$, from the linear region of the $I_{ds}-V_{bgs}$ characteristics (see Figure 8, linear scale). The V_{th} was extracted from the extrapolation to zero of the linear part of the $I_{ds}-V_{bgs}$ characteristics. The subthreshold swing (SS), which is the gate voltage necessary to change the I_{ds} by one decade, was extracted in the range of 10^{-11}A to 10^{-8}A, by $SS = \ln(10)\cdot dV_{bgs}/d\ln(I_{ds})$,[50] from the subthreshold region of the (log) $I_{ds}-V_{bgs}$ characteristics (see Figure 8, log scale). Off-current (I_{off}) and the off-voltage (V_{off}; that is, V_{bgs} of the minimum I_{off} current) were extracted by fitting the $I_{ds}-V_{bgs}$ curve close to the I_{off}.

Transconductance, Carrier Mobility, and Carrier Density. To fully explain the changes in g_m, we used an exponential-approximation for the holes carrier density, Q_S,[2,47,51] rather than the widely used linear approximation[52] (see ref 53 for justification), according to:

$$g_m \propto \mu_h Q_S \tag{3}$$

Since any surface treatment could be regard as molecular gating.[1] The hole carriers mobility, μ_h, of the Si NW FETs can be described by the following relationship:[1,54]

$$\mu_h = \frac{\mu_0}{1 + \left|\frac{1}{\varepsilon_{si}E_0}\left(Q_D + \frac{Q_S}{\eta}\right)\right|^{\gamma}} \tag{4}$$

where Q_D is the depletion charge density, μ_0 is the low field mobility (i.e., the mobility in the absence of applied field), ε_{si} is the silicon permittivity, and γ, η, and E_0 are empirical parameters. Under strong carrier accumulation (above V_{th}), $Q_D \ll Q_S$.[47] Assuming $\gamma = 1$[54] for Si NW and $\varepsilon_{si}E_0\eta$ in the order of the Q_s[55] of the base ($Q_s^0 \approx 1 \times 10^{16}$ cm^{-3}), g_m can be described by the following relationship:

$$g_m \propto \frac{\mu_0 Q_S}{1 + \frac{Q_S}{Q_S^0}} \tag{5}$$

On the basis of eq 5, the change of Q_s of a specific Si NW FET at a backward scan relative to that of the OH^{low}-Si NW FET backward scan ($\Delta Q_S/Q_S^0$), can be described by

$$\frac{\Delta Q_S}{Q_S^0} = \frac{2\Gamma}{1-\Gamma} \tag{6}$$

where $\Gamma = \Delta g_m/g_m^0$ is the change of the g_m of a specific Si NW FET at a backward scan, relative to that of the OH^{low}-Si NW FET backward scan. The change in μ_h of a specific Si NW FET at backward scan relative to the μ_h of the OH^{low}-NW FET backward scan ($\Delta\mu_h/\mu_h^0$), can be described as

Table 3. Relative Changes of the Trans-Conduction ($\Delta g_m/g_m^0$), Carrier Density ($\Delta Q_S/Q_S^0$), Carrier Mobility ($\Delta \mu_h/\mu_h^0$), Threshold Voltage (ΔV_{th}), Threshold Voltage Gap (ΔV_H), off-Current Voltage (ΔV_{off}), Subthreshold Swing (ΔSS), and off-Current (ΔI_{off}) for the Different Si NW FETs or Electrical Scans

	relative change of							
samples/scans comparisons	$\Delta g_m/g_m^0$ (%)	$\Delta Q_S/Q_S^0$ (%)	$\Delta \mu_h/\mu_h^0$ (%)	ΔV_{th} (V)	ΔV_H (V)	ΔV_{off} (V)	ΔSS (V/decade)	ΔI_{off} (pA)
HTS^c-Si NW FET backward scan compared to OH^{low}-Si NW FET backward scan	−41.4	−58.6	+41.4	−0.8		−1	+0.9	-5×10^{-13}
OH^{high}-Si NW FET backward scan compared to OH^{low}-Si NW FET backward scan	+7.6	+16.5	−7.6	+6.7		+5	−3.7	-2.1×10^{-12}
OH^{low}-Si NW FET forward scan compared to OH^{low}-Si NW FET backward scan	−18.0	−31.0	+18.0		−5.7	−8	−0.13	-1.6×10^{-12}
OH^{high}-Si NW FET forward scan compared to OH^{high}-Si NW FET backward scan	−37.2	−54.2	+37.2		−14.7	−33	−1.14	-1×10^{-14}
HTS^c-Si NW FET forward scan compared to HTS^c-Si NW FET backward scan'	−3.3	−6.4	+3.3		−0.8	−1	−0.02	∼0

follows:

$$\frac{\Delta \mu_h}{\mu_h^0} = -\Gamma \tag{7}$$

The superscript "0" in eqs 5−7 stands for the property of the OH^{low}-Si NW FET at the backward scan.

Table 3 shows the calculated $\Delta g_m/g_m^0$, $\Delta \mu_h/\mu_h^0$, and $\Delta Q_S/Q_S^0$ for OH^{high}-Si NW FET and HTS^c-Si NW FET **backward** scans in comparison to the OH^{low}-Si NW FET **backward** scan. As seen in Table 3, the Q_S of the OH^{high}-Si NW FET and HTS^c-Si NW FET **backward** scans increased and decreased, respectively, compared to the OH^{low}-Si NW FET **backward** scan. This could be attributed to the increase of the negatively charged surface states (Q_{css}) of the OH^{high}-Si NW FET and to the decrease of the Q_{css} of the HTS^c-Si NW FET.[2]

The Q_S of all examined Si NW FETs in the **forward** scan were lower than those in the **backward** scan, indicating that the charge sign of Q_{trap} is positive. The implication is that Q_{trap} of the OH^{high}-Si NW FET was higher than that of the OH^{low}-Si NW FET and that the Q_{trap} of the HTS^c-Si NW FET was lower than that of the OH^{high}-Si NW FET.

The discrimination between Q_{trap} to Q_{css} is based on the state dynamics. Q_{css} is referred as ***fast*** (charged) states that do not contribute to the hysteresis, while Q_{trap} is referred as ***slow*** (trap) states that do contribute to the hysteresis.[13,24] These charges change the channel conductivity and screen the applied back-gate field. It has been suggested that charge transfer between the Si NW and the surface Si−OH groups is the major source of Q_{trap}.[13,24] However, our experimental results indicate that the surface Si−OH groups are also the source for Q_{css}.[13,24] Therefore, it is reasonable to assign Q_{trap} to a noncovalent, ***slow*** screening of (part of) the ***fast negative*** Q_{css} (i.e., Si−O$^-$), which is essentially, a formation of ***slow positive*** charge.

To elaborate this analysis we have used the data from Table 3 to evaluate the amount of Q_{trap}, while considering the amount of relevant Q_{css} that were passivated due to the HTS^c modification, using the following modified equations:

$$\frac{[Q_{css}]_{HTS^c}}{[Q_{css}]_{OH^{high}}} = \left(\left[\frac{\Delta Q_S}{Q_S^0}\right]_{HTS^c \rightarrow OH^{low}} + 1\right) \Big/ \left(\left[\frac{\Delta Q_S}{Q_S^0}\right]_{OH^{high} \rightarrow OH^{low}} + 1\right) = \kappa \tag{8}$$

$$\frac{[Q_{trap}]_{HTS^c}}{[Q_{trap}]_{OH^{high}}} = \frac{\left[\frac{\Delta Q_S}{Q_S^0}\right]_{HTS^c F \rightarrow B}}{\left[\frac{\Delta Q_S}{Q_S^0}\right]_{OH^{high} F \rightarrow B}} \cdot \kappa^{-1} \tag{9}$$

where $[Q_{css}]_{HTS^c}$ is Q_{css} of the HTS^c-Si NW FET; $[Q_{css}]_{OH^{high}}$ is Q_{css} of the OH^{high}-Si NW FET; $[Q_{trap}]_{HTS^c}$ is the Q_{trap} of the HTS^c-Si NW FET; and $[Q_{trap}]_{OH^{high}}$ is the Q_{trap} of the OH^{high}-Si NW FET. The subscripts "HTS^c→OH^{low}" and "OH^{high}→OH^{low}" stand for the property of the HTS^c-Si NW FET and OH^{high}-Si NW FET backward scans, respectively, compared to the OH^{low}-Si NW FET backward scan. The superscript "HTS^c F→B" and "OH^{high} F→B" stand for the property of the HTS^c-Si NW FET and OH^{high}-Si NW FET forward scans, respectively, compared to the backward scans. Using eqs 8 and 9, our calculations show that ∼96% of the traps were passivated due to the HTS^c modification. This result is significantly close to the ∼95% estimation that was calculated using the $|\Delta V_H|$ characteristics (see Figure 8).

Subthreshold Swing and Off-Current. The subthreshold swing, SS, is given by the expression[1]

$$SS = \ln(10) \cdot \left(\frac{q}{k_b T} - \frac{1}{E_{bnw} D_{nw}}\right)^{-1} \cdot \left(1 + \frac{C_{it}}{C_{box}} + \frac{C_{si}}{C_{box}}\right) \tag{10}$$

where E_{bnw} is the field at the bottom of the Si NW (i.e., the closest oxide-free Si point to the back SiO_2),[1] D_{nw} is the Si NW diameter, C_{si} is the capacitance of the Si NW, C_{it} is the capacitance of interface states at the SiO_2/Si region of the Si NW, T is the temperature, and k_b is Boltzmann constant. The large decrease observed in the *SS* of OH^{high}-Si NW FET in comparison to the SS of the OH^{low}-Si NW FET (from 6.2 to 2.5 V/decade for the backward scan; see Table 3) could be attributed to a change in the density of interface states (D_{it}) or to a formation of dangling bonds because of the ultraviolet radiation damage (during the UVOCs pretreatment process) of the SiO_2/Si region.[14,56] The increase in the SS of the HTS^c-Si NW FET (from 2.5 to 7.1 V/decade for the backward scan; see Table 3) to a value that is close to the SS of the OH^{low}-Si NW FET (6.2 V/decade for the backward scan; see Table 3) implies that irreversible change in D_{it} could not be the only reason for the SS changes. On the other hand, these changes could be attributed to the formation of Q_{css} when the device is enriched with Si−OH groups and the elimination of Q_{css} when the device is modified with HTS^c. In this case, a large change in Q_{css} might cause significant band bending inside the Si NW that is

expressed by a change in E_{bnw} (ΔE_{bnw}). ΔE_{bnw} can be estimated according to[1]

$$\Delta E_{bnw} = \frac{\frac{\alpha}{D_{nw}}\left(\frac{k_bT}{q}\right)^2 (SS^0 - SS)}{\left(SS - \alpha\frac{k_bT}{q}\right)\left(SS^0 - \alpha\frac{k_bT}{q}\right)} \quad (11)$$

$$\alpha = \ln(10)\cdot\left(1 + \frac{C_{it}}{C_{box}} + \frac{C_{si}}{C_{box}}\right) \quad (12)$$

where SS^0 is the SS of the OH^{low}-Si NW FET backward scan. Our calculations show that a change of about +0.271 V in $E_{bnw}D_{nw}$ decreased the SS of the OH^{high}-Si NW FET by −3.7 V/decade in comparison to the SS of the OH^{low}-Si NW FET and that a change of about −0.273 V in $E_{bnw}D_{nw}$ increased the SS of the HTS^c-Si NW FET by +4.6 V/decade in comparison to the SS of the OH^{high}-Si NW FET. This change in $E_{bnw}D_{nw}$ is larger from the thermal voltage (k_bT/q = 0.026 V), meaning significant changes in the band bending inside the Si NW.

We have recently shown that the band bending inside the Si NW is also expressed in the Schottky barrier (Ψ_b) of the source and drain contacts.[1] It was shown that the higher the band bending, the higher the Ψ_b and the lower the I_{off}. To express the effect of I_{off} (the Schottky thermionic emission current) quantitatively,[57] the following relationship was considered: (cf., refs 57 and 58):

$$I_{off} \propto \exp\left(-\frac{q\Psi_b}{k_bT}\right) \quad (13)$$

According to this relationship, $\Delta\Psi_b$ is given by the expression

$$\Delta\Psi_b = -\frac{k_bT}{q}\ln\left(\frac{I_{off}}{I_{off}^0}\right) \quad (14)$$

where I_{off}^0 is I_{off} of the OH^{low}-Si NW FET backward scan. Our calculations showed that the Ψ_b of OH^{high}-Si NW FET is larger by approximately +0.139 eV than the Ψ_b of the OH^{low}-Si NW FET, leading to a decrease of the I_{off} (from 2.1×10^{-12} Å to a current of the order of 1×10^{-14} Å; see Table 3). The Ψ_b of the HTS^c-Si NW FET is smaller by approximately −0.130 eV, than the Ψ_b of the OH^{high}-Si NW FET, leading to an increase of the I_{off} (back to 1.5×10^{-12}A; see Table 3). This result is consistent with the increase of Q_{css} of the OH^{high}-Si NW FET and to the decrease of Q_{css} of the HTS^c-Si NW FET.

For OH^{low}-Si NW FET and OH^{high}-Si NW FETs, the SS of the I_{ds}-V_{bgs} forward scan was decreased compared to the backward scan (see Table 3).[60] This decrease implies further bending down of the bands.[58−60] This observation is supported by the additional decrease of the I_{off} of the forward scan compared to the backward scan (see Table 3). Interestingly, the changes in SS and I_{off} of the HTS^c-Si NW FET are negligible, *confirming that most of the traps were passivated due to the HTS^c modification*. The band bending inside the Si NW is discussed further below.

Threshold Voltage and Off-Voltage. V_{th} for an accumulation-conduction FET is understood as the V_{bgs} value that corresponds to the onset of significant I_{ds}. At this V_{bgs}, the bottom Si NW surface potential is essentially zero (flat band)[47] and V_{th} is given by the equation[1]

$$V_{th} = V_{FB} - \frac{Q_{box}}{C_{box}} - \frac{Q_D}{C_{box}} \quad (15)$$

where V_{FB} is the difference between the work function of the gate material and of the Si NW, Q_{box} is the sum of all (fixed and trapped) charges in the back oxide of the substrate, including Q_{css} and Q_{trap} at the molecule/back SiO_2 interface and on the Si NW native SiO_2 surface, and Q_D is the absolute charge at the Si NW depletion layer. According to this relationship, ΔV_{th} is given by the expression

$$\Delta V_{th} \approx \frac{q\Delta Q_{css}}{C_{box}} - \frac{\Delta Q_D\{\Delta Q_{css}\}}{C_{box}} \quad (16)$$

where $\Delta Q_D\{\Delta Q_{css}\}$ is the change in the depletion charge density as a result of the change in the negative charged surface states (hereafter, ΔQ_{css}) of the OH^{high}-Si NW FETs or the HTS^c-Si NW FETs backward scans compared to the OH^{low}-Si NW FET backward scan. According to eq 16, the large increase in Q_{css} of the OH^{high}-Si NW FET in comparison to the Q_{css} of the OH^{low}-Si NW FET ($\Delta Q_{css} > 0$) leads to a positive shift of the V_{th} of the OH^{high}-Si NW FET backward scan compared to the V_{th} of the OH^{low}-Si NW FET backward scan (ΔV_{th} = +6.7 V, see Table 3). The large decrease in Q_{css} of the HTS^c-Si NW FET compared to the Q_{css} of the OH^{high}-Si NW FET ($\Delta Q_{css} <$ 0), leads to a negative shift of the V_{th} of the HTS^c-Si NW FET backward scan compared to the V_{th} of the OH^{high}-Si NW FET backward scan (ΔV_{th} = −7.5 V; see Table 3).

According to the relationship of eq 15, ΔV_H is given by the expression

$$\Delta V_H \approx -\frac{qQ_{trap}}{C_{box}} - \frac{\Delta Q_D\{Q_{trap}\}}{C_{box}} \quad (17)$$

where $\Delta Q_D\{Q_{trap}\}$ is the change in the depletion charge density as a result of the change in the Q_{trap} of a specific sample in its forward scan relative to its backward scan. According to eq 17, the ΔV_H was negative for each of the I_{ds}−V_{bgs} characteristics of the examined samples, implying that the charge sign of Q_{trap} is positive, in consistency with our conclusions from the g_m analysis. **Note:** assuming that ΔQ_{css} or Q_{trap} everywhere on the SiO_2 surface of the Si NW FET (cf. Figure 4) is nearly balanced by a mirror image charge,[59] this might lead to a considerable change in Q_D (second order change) (cf. also refs 12 and 14).

As regards to the V_{off}, we have recently shown that the higher the E_{bnw}, the higher the value of V_{th} (negative) that is needed to reach the accumulation mode.[1] Additionally, we have shown that the higher the E_{bnw}, the lower the value of V_{off} (positive) that is needed to reach the minimum current. In fact, the change in V_{off} (ΔV_{off}) and ΔV_{th} or ΔV_H should be of the same order of magnitude and should follow similar trends.[1] As seen in Table 3, the ΔV_H and/or ΔV_{th}, follow this notion.

Hysteresis versus Back-Gate Voltage. The total backward conductivity (G_B) and forward conductivity (G_F) of the Si NW FETs could be expressed through the following model:[2]

$$G_B = q\mu_h^B\left(Q_S^v(V_{gs} - V_{th}^B) + \frac{2Q_{css}}{r_{nw}}\right)L_{nw} \quad (18)$$

$$G_F = q\mu_h^F\left(Q_S^v(V_{gs} - V_{th}^F) + \frac{2Q_{css}}{r_{nw}} - \frac{2Q_{trap}}{r_{nw}}\right)L_{nw} \quad (19)$$

where V_{th}^B and V_{th}^F are the V_{th} of the backward and forward scans, respectively; μ_h^B and μ_h^F are the μ_h of the backward and forward scans, respectively; Q_S^v is the volume density of holes that origin from applying back-gate voltage; $2Q_{scc}/r_{nw}$ and

$2Q_{trap}/r_{nw}$ are the surface induced holes that origin from Q_{css} and Q_{trap}, respectively. **Note:** for HTS^c we assume that each negative (positive) surface charge would contribute a hole (electron) to the Si NW and that small Q_{trap} (or Q_{css}) gives rise to a small change in the FET characteristics. On the basis of eqs 18 and 19, the relative conductivity change of the forward scan compared to the backward scan, $(G_F - G_B)/G_B$, as a function of V_{bgs} could be formulated as follows:

$$\frac{G_F - G_B}{G_B} \approx \frac{-1}{\frac{r_{nw}}{2}\frac{Q_S^v(V_{bgs} - V_{th}^B)}{Q_{css}} + 1} \cdot \frac{\mu_h^F}{\mu_h^B}\frac{Q_{trap}}{Q_{css}} \quad (20)$$

As seen in eq 20, the $(G_F - G_B)/G_B$ is composed of two parts. The first part is a prefactor (PF) that includes the ratio between Q_S^v and Q_{css}. The second part presents the ratio between Q_{trap} and Q_{css}. Figure 11 shows the $(G_F - G_B)/G_B$ versus V_{bgs} and

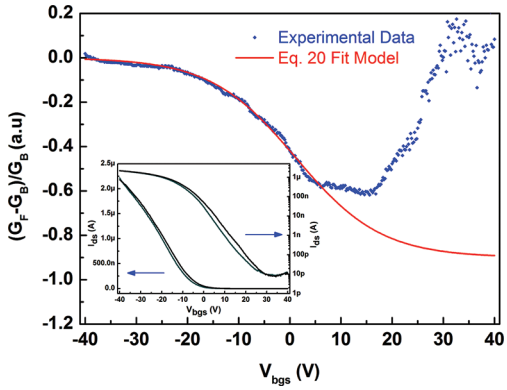

Figure 11. $(G_F - G_B)/G_B$ vs V_{bgs} calculated from the I_{ds}–V_{bgs} characteristics seen in the inset and fit curve based on eq 20. **Inset:** Linear scale (left axis) and Log scale (right axis) scale forward and backward I_{ds}–V_{bgs} characteristics of representative HTS^c-Si NW FET response under 15% RH. $(G_F - G_B)/G_B$ was calculated according to $(G_F - G_B)/G_B = (I_{ds}^F - I_{ds}^B)/I_{ds}^B$, where I_{ds}^F and I_{ds}^B are I_{ds} of the backward and forward scans, respectively.

the curve fitted according to eq 20. As seen in the figure, at high negative gate voltage the relative change in conductivity (the PF → 0) approaches zero. Applying more positive gate voltage reduces the PF exponentially. According to this model, at high negative back-gate voltage, PF → −1, namely, Q_{trap} is demonstrated most efficiently in the high positive gate voltage, where the devices are almost turned off.[2] However, at ∼5 V, the exponential shape is changed and at ∼15 V, the relative conductivity change is increased back to zero. At high positive V_{bgs}, particularly at V_{off}, where the device turns to its off state, the I_{ds} is no longer governed by the total hole density, but rather is limited by tunneling through the Ψ_b of the contact.[58] Therefore, the conductivity in the Si NW FET at this region could be expressed through

$$G \propto \exp\left(-\frac{q\Psi_b}{k_bT}\right) \quad (21)$$

and $(G_F - G_B)/G_B$ could be formulated as follows:

$$\frac{G_F - G_B}{G_B} \approx \exp\left(-\frac{q\Delta\Psi_b}{k_bT}\right) - 1 \quad (22)$$

It has been shown recently that Ψ_b at the source contact of p-type Si NW FET is increased at positive V_{bgs}.[57] However, at a point near the V_{off}, $\Delta\Psi_b$ approaches zero, because the maximum band bending of the forward and backward scans is reached. For any higher positive V_{bgs}, $(G_F - G_B)/G_B$ is zero, with characteristic noise that originates from I_{ds} of the order of <10 pA that is used to calculate $(G_F - G_B)/G_B$.

Interestingly, based on eq 20, the exponential fit curve is saturated at high positive V_{bgs} on a value of −0.9 $(\mu_h^F Q_{trap}/\mu_h^B Q_{css})$. This observation implies that under 15% RH, 86% of the negative Q_{css} are screened to induce positive Q_{trap}. Similar model-based analysis could be done for OH^{high}-Si NW FET and HTS^c-Si NW FETs compared to OH^{low}-Si NW FET or for the forward scan compared to the backward scan. In this case, a large change in Q_{trap} and Q_{css} gives rise to a large change in the FET characteristics (see Supporting Information, eq 1S–4S).

Hysteresis Effect on Sensing. The limited sensitivity of the HTS^{uc}-Si NW FET sensors toward nonpolar analytes under real-world environment is attributed, predominantly, to the hysteresis drift. Over time, free (uncreacted) Si–OH groups, molecule-free sites and nanometric pinholes of the HTS^{uc}-Si NW surface are directly occupied (see Figure 4b, right side), by all sorts of atmospheric analytes (most effectively by polar ones because of the hydrophilic nature of SiO_2). This essentially gives rise to a hysteresis drift that screens the sensing signal of the target nonpolar analytes and to a limited sensitivity.[2]

The sensing results of the HTS^c-Si NW FETs shown in Figure 9 are consistent with the notion that HTS^c modification passivates most of the Q_{trap}. The formation of a dense hydrophobic HTS^c monolayer acts to increase the recognition of noninteracting nonpolar analytes (hydrophobic monolayer vs hydrophilic SiO_2 surfaces) while preventing polar analytes from reaching the remaining Si–OH groups on the Si NW FET oxide surface. Consequently, the hysteresis drift and the sensitivity of the HTS^c-Si NW FET in response to polar analytes are significantly reduced, while the sensitivity to nonpolar analytes is dramatically increased with no hysteresis drift.

The humidity dependence shown in Figure 10 is consistent with the proposed relation between Q_{css} and Q_{trap}. At low humidity levels, water molecules act to screen the remaining Q_{css} and to form Q_{trap}, thus saturating the ΔV_H. This mechanism is consistent with the result that only 86% of Q_{css} is screened by water molecules, proning the rest of Q_{css} for screening under a higher humidity levels (cf., Figure 11 and Hysteresis versus Back-Gate Voltage section). At high humidity levels, a thin film of water is formed on the surface. Thus, a water mediation of charge transfer to and from the traps could explain the higher but fixed ΔV_H.[13,18]

The responses of the HTS^c-Si NW FET backward scan toward the different RH conditions and polar analytes are important observations in Figures 9 and 10. The backward scan is noted without the effect of the trapped charge. Therefore, any response in the backward scan is attributed to other effects of water and polar analytes, such as dipole or dielectric effects (cf., ref 2 for more details). The negligible response of the HTS^c-Si NW FET backward scan in the subthreshold region to polar analytes (see Figures 9 and 10) implies the ability to detect nonpolar analytes in a complex solution containing high levels of RH and polar analytes (see Figure 9, log scale). The small and negligible hysteresis drift of HTS^c-Si NW FET in response to polar and nonpolar analytes, respectively, could be used as a feature to differentiate between polar and nonpolar analytes.

SUMMARY AND CONCLUSIONS

In this study, we propose that the hydrophobicity or molecular density criteria used to evaluate the quality of the (TS) monolayer for surface passivation purposes are not necessarily useful to evaluate the quality of the Si NW gas sensors. Rather, we propose that the critical criterion for the evaluation of sensing performances of Si NWs is the concentration of the exposed or unpassivated hydroxyl (Si−OH) groups (trap states) within the adsorbed tricholorosilane (TS) monolayer. Following this notion, we have shown that elimination of the free (unreacted) Si−OH groups adsorbed on the Si NW surface by a TS^c adsorption process improves both the electrical and sensing properties of the Si NW FETs. Such improvements were expressed via a decrease in the hysteresis magnitude and hysteresis drift of the Si NW FET on exposure to (polar or nonpolar) analytes as well as to humidity at different concentration levels. Additional improvements due to the TS^c adsorption were expressed through a decrease in the sensitivity of the Si NW FETs to polar analytes and through an increase in the sensitivity of the Si NW FETs to nonpolar analytes. Failure to eliminate (part of) the free (unreacted) Si−OH groups from the Si NWs, as is the case with the bare Si NW FETs or with the Si NW FETs coated with TS^{uc}, severely damage the electrical and sensing performance of the device. Neither low packing nor high packing densities of the TS^{un} can fairly eliminate the Si−OH groups on the (native) SiO_2-coated Si surface.

Model-based analysis of the Si NW FETs indicated that the hysteresis effect increases the carrier mobility (μ_h), decreases the subthreshold swing (SS), decreases the off-current (I_{off}), shifts the threshold voltage (V_{th}) to negative gate voltages, and shifts the off voltage (V_{Ioff}) to negative gate voltages. The model-based analysis indicates further that the hysteresis effect *per se* originates from ***positively*** charged ***slow*** trap states (Q_{trap}) that are formed by a screening of ***negatively*** charged ***fast*** states (Q_{css}), which are associated with surface Si−OH groups. Enrichment of Si NW FETs by Si−OH groups, therefore, increases the hysteresis effect substantially. On the other hand, eliminating most of the Si−OH groups by HTS^c decreases the hysteresis effect dramatically.

Overall, this work implies that proper chemical passivation of the Si−OH groups on the Si NW surface could serve to achieve stable and reproducible Si NW FET-based gas sensors under real-world humidity conditions. Achieving Si sensors with a variety of termination groups, while preserving the passivation of the Si−OH groups, can be accomplished by subsequent reaction or modification (cf. refs 31 and 61−64) of the TS^c with the desired chemical functionalities. These surfaces can then be used for discrimination between polar and nonpolar analytes in complex, real-world gas mixtures by considering the Si NW FET backward scan and/or the magnitude of hysteresis per se.

ASSOCIATED CONTENT

Supporting Information

Extended model supported analysis for hysteresis versus back-gate voltage, XPS C_{1s} and Si_{2p} spectra of different TS^c coated planar Si(111) surfaces, forward and backward $I_{ds}-V_{bgs}$ characteristics of OH^{low}-Si NW FET and HTS^{uc}-Si NW FETs over ∼10 h exposure, HTS^c-Si NW FETs over ∼2 h exposure under 15% RH and scheme for the direct self-assembly procedure. This material is available free of charge via the Internet at http://pubs.acs.org.

AUTHOR INFORMATION

Corresponding Author

*E-mail: hhossam@technion.ac.il.

Notes

The authors declare no competing financial interest.

ACKNOWLEDGMENTS

The research leading to these results has received funding from the FP7-Health Program under the LCAOS (grant agreement no. 258868). We acknowledge Dr. Silke Christiansen (Max Planck Institute for the Science of Light) and Dr. Thomas Stelzner for supplying part of the Si NWs, Mr. Ossama Assad (Technion) for assistance with the SEM image and Dr. Dory Cwikel (Technion) for assistance with contact angle measurements. H.H. is a Knight of the Order of Academic Palms.

NOMENCLATURE

Abbreviations and Acronyms

FET = field effect transistor
HTS = hexyltrichlorosilane
NW = nanowire
OTS = octadecyltrichlorosilane
PF = prefactor
ppb = parts per billion
ppm = parts per million
PTS = propyltrichlorosilane
RH = relative humidity
SEM = scanning electron microscopy
TEM = transmission electron microscopy
Ti = titanium
TMA = trimethylamine
TS = trichlorosilane
TSAPR = two-step amine-promoted reaction
UV-NIR = ultraviolet−near infrared
UVOCs = ultraviolet ozone cleaning
XPS = X-ray photoelectron spectroscopy

Symbols

$2Q_{css}/r_{nw}$ = induced holes that origin from negative charged surface states
$2Q_{trap}/r_{nw}$ = induced holes that origin from occupied trap charges on the surface
Au = gold
C = carbon
C 1s = carbon 1s XPS spectrum
C 1s C−C = carbon-type C−C XPS peak
C 1s C−O = carbon-type C−O XPS peak
C_{box} = capacitance of the FET's gate oxide
C−C = carbon−carbon bond
C_{it} = capacitance of interface states at the SiO_2/Si region
C_{Si} = capacitance of the silicon core in the Si NW
d_{box} = thickness of the FET's back gate oxide
D_{it} = density of the interface states
D_{nw} = diameter of the Si NW
d_{TS} = thickness of the trichlorosilane monolayer
E_0 = empirical parameter
E_{bnw} = field at the bottom of the Si NW
F → B = specific property that is measured or extracted in the forward scan, compared to the same property in the backward scan
G = conductivity
G_B = conductivity of the Si NW FET in the backward scan
G_F = conductivity of the Si NW FET in the forward scan

g_m = transconductance
g_m^0 = transconductance of a reference sample
H_2O = water
HTS^c = controlled, TSAPR-made hexyltrichlorosilane monolayer
HTS^c-Si NW FET = field effect transistor with silicon nanowire channel that is coated with TSAPR-made hexyltrichlorosilane monolayer
HTS^{uc} = hexyltrichlorosilane monolayer prepared by the direct self-assembly procedure
HTS^{uc}-Si NW FET = field effect transistor with silicon nanowire channel with hexyltrichlorosilane monolayer that is prepared by the direct self-assembly procedure
I_{ds} = source-drain current
I_{ds}^B = source-drain current of the backward scan
I_{ds}^F = source-drain current of the forward scan
I_{off} = off-current
I_{off}^0 = off-current of the reference sample
k = dielectric constant
k_b = Boltzmann constant
k_bT/q = thermal voltage
L_{nw} = length of the Si NW
n = refractive index
n_∞ = electronic part of the refractive index
$n(\lambda)$ = wavelength-dependent refractive index
OH = hydroxyl group
OH^- = hydroxyl ion
OH^{high}-Si NW FET = field effect transistor with OH-enriched silicon nanowire surface (after UVOCs treatment)
OH^{low}-Si NW FET = field effect transistor with no UVOCs pretreatment of the silicon nanowire surface
OTS^c = controlled, TSAPR-made octadecyltrichlorosilane
OTS^{uc} = octadecyltrichlorosilane monolayer prepared by the direct self-assembly procedure
PTS^c = controlled, TSAPR-made propyltrichlorosilane monolayer
q = elementary charge of electron
Q_{box} = sum of all fixed and trapped charges in the back oxide of the substrate
Q_{css} = negative charged surface states
$[Q_{css}]^c_{HTS}$ = negative charged surface states of a field effect transistor with silicon nanowire channel that is coated with TSAPR-made hexyltrichlorosilane monolayer
$[Q_{css}]^{high}_{OH}$ = negative charged surface states of a field effect transistor with OH-enriched silicon nanowire surface (after UVOCS treatment)
Q_D = depletion charge density
Q_S = carrier charge density
Q_S^0 = carrier charge density of a reference sample
Q_S^v = volume density of carrier charges
Q_{trap} = number of occupied trap charges
$[Q_{trap}]^c_{HTS}$ = number of occupied trap charges of a field effect transistor with silicon nanowire channel that is coated with TSAPR-made hexyltrichlorosilane monolayer
$[Q_{trap}]^{high}_{OH}$ = number of occupied trap charges of a field effect transistor with OH-enriched silicon nanowire surface (after UVOCS treatment)
r_C = ratio between the XPS's C_{1s} C−C and Si_{2p} SiO_2 peak areas
r_{nw} = radius of the Si NW
$r_{R\text{-}SiO3}$ = ratio between the XPS's Si_{2p} R-SiO_3 and Si_{2p} SiO_2 peak areas
$r_{Si3/2}$ = ratio between the XPS's Si $2p_{3/2}$ and Si_{2p} SiO_2 peak areas
R-SiO_3 = surface bound trichlorosliane molecule
Si^{2+} = highly doped silicon
Si2p1/2 = bulk silicon-type 1/2 XPS peak
Si2p3/2 = bulk silicon-type 3/2 XPS peak
Si_{2p} = silicon 2p XPS spectrum
Si2p R-SiO_3 = surface silicon-type R-SiO_3 XPS peak
Si2p Si_2O = surface silicon-type Si_2O XPS peak
Si2p Si_2O_3 = surface silicon-type Si_2O_3 XPS peak
Si2p SiO = surface silicon-type SiO XPS peak
Si2p SiO_2 = surface silicon-type SiO_2 XPS peak
Si−C = silicon−carbon bond
$Si-O^-$, $Si-OH_2^+$ = oxide surface ionic species
SiO_2 = silicon dioxide
Si−OH = surface hydroxyl group
Si−O−Si = silicon−oxygen-silicon bond
SiO_x-Si(111) = planar silicon (111) coated with native silicon oxide
SS = subthreshold swing
SS^0 = subthreshold of a reference sample
TS^c = controlled, TSAPR-made trichlorosilane monolayer
TS^{uc} = trichlorosilane monolayer prepared by the direct self-assembly procedure
TS^c-Si(111) = planar silicon (111) coated with TSAPR-made trichlorosilane
TS^c-Si NW FET = field effect transistor with silicon nanowire channel that is coated with TSAPR-made trichlorosilane monolayer
TS^{uc}-Si NW FET = field effect transistor with silicon nanowire channel with trichlorosilane monolayer that is prepared by the direct self-assembly procedure
V_{bgs} = back gate voltage
V_{ds} = source-drain voltage
V_{FB} = flat band voltage, that is, the difference between the gate material and the silicon nanowire work function
ΔV_H = gap of threshold voltage
V_{off} = off-voltage
V_{th} = threshold voltage
V_{th}^B = threshold voltage in the backward scan
V_{th}^F = threshold voltage in the forward scan

Greek Symbols

α = ratio between all the capacitances to the back oxide capacitance in the silicon nanowire field effect transistor
γ = empirical parameter
Δ = change or shift of a specific property
ε_{box} = dielectric constant of the back oxide of the silicon nanowire field effect transistor
ε_{si} = dielectric constant of the silicon core of the silicon nanowire
ε_{TS} = dielectric constant of TSAPR-made trichlorosilane monolayer
η = empirical parameter
θ_{TS} = contact angle of planar silicon (111) coated with TSAPR-made trichlorosilane
λ = wavelength
μ_0 = low field mobility
μ_h = hole mobility
μ_h^0 = hole mobility of a reference sample
μ_h^B = hole mobility in a backward scan
μ_h^F = hole mobility in a forward scan
Γ = relative change of the trans-conductance
κ = ratio between the negative charged surface states of the controlled, TSAPR-made hexyltrichlorosilane monolayer and

the negative charged surface states of OH-enriched silicon nanowire surface (after UVOCS treatment)
Φ_{Au} = work function of gold
$\Phi_{TS\text{-}Si(111)}$ = work function of planar silicon (111) coated with TSAPR-made trichlorosilane
Ψ_b = Schottky barrier of the source or drain contact

REFERENCES

(1) Paska, Y.; Stelzner, T.; Assad, O.; Tisch, U.; Christiansen, S.; Haick, H. *ACS Nano* **2012**, *6*, 335−345.
(2) Paska, Y.; Stelzner, T.; Christiansen, S.; Haick, H. *ACS Nano* **2011**, *5*, 5620−5626.
(3) Tisch, U.; Haick, H. *MRS Bull.* **2010**, *35*, 797−803.
(4) Ahn, J.-H.; Choi, S.-J.; Han, J.-W.; Park, T. J.; Lee, S. Y.; Choi, Y.-K. *Nano Lett.* **2010**, *10*, 2934−2938.
(5) Ramgir, N. S.; Yang, Y.; Zacharias, M. N. *Small* **2010**, *6*, 1705−1722.
(6) Stern, E.; Vacic, A.; Reed, M. A. *IEEE Trans. Electron. Dev.* **2008**, *55*, 3119−3130.
(7) McAlpine, M. C.; Ahmad, H.; Wang, D.; Heath, J. R. *Nat. Mater.* **2007**, *6*, 379−384.
(8) Cui, Y.; Wei, Q.; Park, H.; Lieber, C. M. *Science* **2001**, *293*, 1289−1292.
(9) Lee, J. W.; Jang, D.; Kim, G. T.; Mouis, M.; Ghibaudo, G. *J. Appl. Phys.* **2010**, *107*, 044501/1−044501/4.
(10) Bashouti, M. Y.; Tung, R. T.; Haick, H. *Small* **2009**, *5*, 2761−2769.
(11) Haight, R.; Sekaric, L.; Afzali, A.; Newns, D. *Nano Lett.* **2009**, *9*, 3165−3170.
(12) Schmidt, V.; Wittemann, J. V.; Senz, S.; Goesele, U. *Adv. Mater.* **2009**, *21*, 2681−2702.
(13) Jie, J.; Zhang, W.; Peng, K.; Yuan, G.; Lee, C. S.; Lee, S.-T. *Adv. Funct. Mater.* **2008**, *18*, 3251−3257.
(14) Schmidt, V.; Senz, S.; Goesele, U. *Appl. Phys. A* **2007**, *86*, 187−191.
(15) Leu, P. W.; Shan, B.; Cho, K. *Phys. Rev. B.* **2006**, *73*, 195320.
(16) Jang, H.; Lee, J.; Lee, J. H.; Seo, S.; Park, B.-G.; Kim, D. M.; Kim, D. H.; Chung, I.-Y. *Appl. Phys. Lett.* **2011**, *99*, 252103.
(17) Kawashima, T.; Saitoh, T.; Komori, K.; Fujii, M. *Thin Solid Films* **2009**, *517*, 4520−4526.
(18) Fahem, Z.; Csaba, G.; Erlen, C. M.; Lugli, P.; Weber, W. M.; Geelhaar, L.; Riechert, H. *Phys. Stat. Sol. C* **2008**, *5*, 27−30.
(19) Colli, A.; Fasoli, A.; Ronning, C.; Pisana, S.; Piscanec, S.; Ferrari, A. C. *Nano Lett.* **2008**, *8*, 2188−2193.
(20) Colli, A.; Fasoli, A.; Beecher, P.; Servati, P.; Pisana, S.; Fu, Y.; Flewitt, A. J.; Milne, W. I.; Robertson, J.; Ducati, C.; De Franceschi, S.; Hofmann, S.; Ferrari, A. C. *J. Appl. Phys.* **2007**, *102*, 034302−13.
(21) Weber, W. M.; Geelhaar, L.; Graham, A. P.; Unger, E.; Duesberg, G. S.; Liebau, M.; Pamler, W.; ChÃze, C.; Riechert, H.; Lugli, P.; Kreupl, F. *Nano Lett.* **2006**, *6*, 2660−2666.
(22) Byon, K.; Tham, D.; Fischer, J. E.; Johnson, A. T. *Appl. Phys. Lett.* **2005**, *87*, 193104.
(23) Cahen, D.; Naaman, R.; Vager, Z. *Adv. Funct. Mater.* **2005**, *15*, 1571−1578.
(24) Lee, J. S.; Ryu, S.; Yoo, K.; Choi, I. S.; Yun, W. S.; Kim, J.-S. *J. Phys. Chem. C* **2007**, *111*, 12504−12507.
(25) Konvalina, G.; Haick, H. *ACS Appl. Mater. Interf.* **2012**, *4*, 317−325.
(26) Tisch, U.; Haick, H. *Rev. Chem. Eng.* **2011**, *26*, 171−179.
(27) Hair, M. L.; Tripp, C. P. *Coll. Surf. A* **1995**, *105*, 95−103.
(28) Tripp, C. P.; Hair, M. L. *Langmuir* **1992**, *8*, 1120−1126.
(29) Tripp, C. P.; Hair, M. L. *Langmuir* **1992**, *8*, 1961−1967.
(30) Haick, H.; Hurley, P.; Hochbaum, A. I.; Yang, P.; Lewis, N. S. *J. Am. Chem. Soc.* **2006**, *128*, 8990−8991.
(31) Assad, O.; Puniredd, S. R.; Stelzner, T.; Christiansen, S.; Haick, H. *J. Am. Chem. Soc.* **2008**, *130*, 17670−17671.
(32) Calhoun, M. F.; Sanchez, J.; Olaya, D.; Gershenson, M. E.; Podzorov, V. *Nat. Mater.* **2008**, *7*, 84−89.
(33) Gao, X. P. A.; Zheng, G.; Lieber, C. M. *Nano Lett.* **2010**, *10*, 547−552.
(34) Li, J.; Zhang, Y.; To, S.; You, L.; Sun, Y. *ACS Nano* **2011**, *5*, 6661−6668.
(35) Ohtake, T.; Mino, N.; Ogawa, K. *Langmuir* **1992**, *8*, 2081−2083.
(36) Wasserman, S. R.; Tao, Y. T.; Whitesides, G. M. *Langmuir* **1989**, *5*, 1074−1087.
(37) Paska, Y.; Haick, H. *J. Phys. Chem. C* **2009**, *113*, 1993−1997.
(38) Tripp, C. P.; Hair, M. L. *J. Phys. Chem.* **1993**, *97*, 5693−5698.
(39) Stelzner, T.; Andra, G.; Wendler, E.; Wesch, W.; Scholz, R.; Goesele, U.; Christiansen, S. *Nanotechnology* **2006**, *17*, 2895−2898.
(40) Paska, Y.; Haick, H. *Appl. Phys. Lett.* **2009**, *95*, 233103/1−233103/3.
(41) Paska, Y.; Haick, H. *J. Am. Chem. Soc.* **2010**, *132*, 1774−1775.
(42) Cwikel, D.; Zhao, Q.; Liu, C.; Su, X.; Marmur, A. *Langmuir* **2010**, *26*, 15289−15294.
(43) Bashouti, M. Y.; Paska, Y.; Puniredd, S. R.; Stelzner, T.; Christiansen, S.; Haick, H. *Phys. Chem. Chem. Phys.* **2009**, *11*, 3845−3848.
(44) Bashouti, M. Y.; Stelzner, T.; Berger, A.; Christiansen, S.; Haick, H. *J. Phys. Chem. C* **2008**, *112*, 19168−19172.
(45) Bashouti, M. Y.; Stelzner, T.; Berger, A.; Christiansen, S.; Haick, H. *J. Phys. Chem. C* **2009**, *113*, 14823−14828.
(46) Kar, S.; Vijayaraghavan, A.; Soldano, C.; Talapatra, S.; Vajtai, R.; Nalamasu, O.; Ajayan, M. P. *Appl. Phys. Lett.* **2006**, *89*, 132118/1−132118/3.
(47) Sze, S. M., *Semiconductor Devices: Physics and Technology*, 2nd ed.; John Wiley & Sons, Inc.: Chichester, U.K., 2001; p 568.
(48) Fleetwood, D. M. *IEEE Trans. Nucl. Sci.* **1992**, *39*, 269−271.
(49) Fleetwood, D. M. *IEEE Trans. Nucl. Sci.* **1996**, *43*, 779−786.
(50) Hovel, H. J. *Sol. St. Elec.* **2003**, *47*, 1311−1333.
(51) Khanal, D. R.; Levander, A. X.; Yu, K. M.; Liliental-Weber, Z.; Walukiewicz, W.; Grandal, J.; Sanchez-Garcia, M. A.; Calleja, E.; Wu, J. *J. Appl. Phys.* **2011**, *110*, 033705.
(52) Wunnicke, O. *Appl. Phys. Lett.* **2006**, *89*, 083102.
(53) Generally, g_m is used to calculate the holes mobility (μ_h) with the following common formalism: $\mu_h = g_m L_{nw}^2 / C_{box} V_{ds}$. The basic assumption of this formalism is a linear relation of the carrier charge density, Q_S (linear-approximation: $Q_S \propto C_{box}[V_{bgs} - V_{th}]$). Using this approach, we have recently presented calculations for the change in μ_h in response to a change in the negative surface charge density, assuming small changes in Q_S (see refs 1 and 2). However, for large changes in Q_S, such as seen in the I_{ds}−V_{bgs} curves of the OH^{high}-Si NW FET and HTS^{c}-Si NW FET (Figure 8), in comparison to the OH^{low}-Si NW FET, a change in μ_h cannot solely explain the changes in g_m. For example, g_m (or μ_h) of the HTS^{c}-Si NW FET backward scan is 59% of the g_m (or μ_h) of the OH^{low}-Si NW FET backward scan. This observation stands in contradiction to the expectation that a large decrease in Q_S should give rise to large increase in μ_h because of reduction of surface and bulk carrier scattering effects.
(54) Choi, L.; Hong, B. H.; Jung, Y. C.; Cho, K. H.; Yeo, K. H.; Kim, D.-W.; Jin, G. Y.; Oh, K. S.; Lee, W.-S.; Song, S.-H.; Rieh, J. S.; Whang, D. M.; Hwang, S. W. *IEEE Elect. Dev. Lett.* **2009**, *30*, 665−667.
(55) The "relative" terms and/or values are used to extract quantitatively the magnitude and direction of the fundamental changes without considering the absolute values of each empirical parameter.
(56) Cernusca, M.; Heer, R.; Reider, G. A. *Appl. Phys. B* **1998**, *66*, 367−370.
(57) Zaremba-Tymieniecki, M.; Durrani, Z. A. K. *Appl. Phys. Lett.* **2011**, *98*, 102113.
(58) Koo, S.-M.; Edelstein, M. D.; Li, Q.; ARichter, C.; Vogel, E. M. *Nanotechnology* **2005**, *16*, 1482−1485.
(59) Assuming that Q_{trap} and ΔQ_{css} are nearly or partially balanced by a mirror image mobile charge inside the Si NW. Mirror image charge is defined as the sum of ΔQ_s, ΔQ_D, and ΔQ_{it} of both the Si NW and substrate that cancel out ΔQ_{css} and Q_{trap} to the first order.
(60) When considering hysteresis, changes in D_{it} cannot be ruled out. This is because positive Q_{trap} on the Si NW surface might decrease D_{it}, and, consequently, decreases SS and bent the bands further.

(61) Puniredd, S. R.; Assad, O.; Haick, H. *J. Am. Chem. Soc.* **2008**, *130*, 9184−9185.
(62) Puniredd, S. R.; Assad, O.; Haick, H. *J. Am. Chem. Soc.* **2008**, *130*, 13727−13734.
(63) Puniredd, S. R.; Assad, O.; Stelzner, T.; Christiansen, S.; Haick, H. *Langmuir* **2011**, *27*, 4764−4771.
(64) Puniredd, S. R.; Platzman, I.; Tung, R. T.; Haick, H. *J. Phys. Chem. C.* **2010**, *114*, 18674−18678.